Reducing theoretical uncertainties for exclusive Higgs-boson plus one-jet production at the LHC

Xiaohui Liu and Frank Petriello

Phys. Rev. D **87**, 094027 — Published 29 May 2013

DOI: 10.1103/PhysRevD.87.094027

ANL-HEP-PR-13-16

Reducing theoretical uncertainties for exclusive Higgs plus one-jet production at the LHC

Xiaohui Liu[1,2,*] and Frank Petriello[1,2,†]

[1]*High Energy Physics Division, Argonne National Laboratory, Argonne, IL 60439, USA*

[2]*Department of Physics & Astronomy,*
Northwestern University, Evanston, IL 60208, USA

Abstract

We resum a class of large Sudakov logarithms affecting Higgs boson production in the exclusive one-jet bin at the LHC. We extend previous results by calculating the full one-loop soft function for this process, which extends the accuracy of the resummation to include the leading three logarithmic corrections at each order in the QCD coupling constant. We match this result to the next-to-leading order cross section and present a detailed numerical study assuming realistic LHC cuts. Careful attention is paid to the matching procedure, and to the theoretical uncertainties induced by residual scale variation. We find that the matched NLL$'$ + NLO cross section has significantly smaller uncertainties than the fixed-order result, and can be used to alleviate the theoretical errors hindering current Higgs analyses at the LHC.

*xiaohui.liu@northwestern.edu

†f-petriello@northwestern.edu

I. INTRODUCTION

The discovery last year of a new boson by the ATLAS and CMS collaborations at the LHC [1, 2] has ushered in a new era in particle physics. The future program of the LHC, and the next stage of experimental studies in high energy physics, will be largely devoted to measuring and understanding the properties of the new state in order to determine the underlying theory from which it arises. The initial data provides only a hazy glimpse at the properties of the new particle. Initial measurements of its branching ratios into various final states indicates that its couplings are consistent with those predicted for the Standard-Model Higgs boson [3], as is its parity [4]. Significant work will clearly be needed to sharpen our picture of the new state.

A major component of the quest for a better understanding of the newly-discovered state will be the improvement of theoretical predictions for Higgs-boson production and decay channels. It is well-known that the next-to-leading order (NLO) QCD radiative corrections to the gluon-initiated $gg \to H + X$ production process are so large [5–11] that next-to-next-to-leading order (NNLO) results are required to realistically describe LHC measurements. NNLO calculations are available for inclusive Higgs boson production [12–14] and for the fully-differential Higgs plus zero-jet cross section [15–19]. Recently, first results for the NNLO cross section in the Higgs plus one-jet channel have become available [20]. As the gluon-fusion process is the primary production mode at the LHC, it has received an enormous amount of theoretical attention. In addition to the QCD corrections through NNLO, the leading electroweak [21, 22] and mixed QCD-electroweak [23] corrections are known. More complete recent reviews of precision predictions for the gluon-fusion and other production channels can be found in Refs. [24–27].

Most of the theoretical predictions described above are obtained using fixed-order perturbation theory, and assume that there are no severe cuts on the phase space of the hadronic radiation produced in association with the Higgs. Unfortunately, such constraints are present in several important Higgs search channels. A well-known example is that of a Higgs boson decaying to W-bosons [28, 29]. The background composition to this signal changes as a function of jet multiplicity. In the zero-jet bin the background is dominated by continuum WW production, while in the one-jet and two-jet bins, top-pair production becomes increasingly important. The optimization of this search requires cuts dependent on the number

of jets observed, and therefore also on theoretical predictions for exclusive jet multiplicities. Theoretical predictions for exclusive jet bins suffer from large logarithms of the form $L = \ln(Q/p_T^{veto})$, where $Q \sim M_H$ denotes the hard scale in the process. For disparate scales Q and p_T^{veto}, these logarithms can overcome the α_s suppression that occurs at each order in perturbation theory, and fixed-order results can consequently lead to incorrect conclusions. For example, for the experimentally relevant values $p_T^{veto} \sim 25 - 30$ GeV, residual scale variations in fixed-order calculations lead to estimated errors that do not accurately reflect uncalculated higher-order corrections [30–32]. The importance of controlling these large logarithms in order to obtain reliable central values and uncertainties for the gluon-fusion channel in exclusive jet bins has been emphasized in the literature [32–34].

The theoretical community has invested significant recent effort in attempting to resum jet-veto logarithms to all orders in perturbation theory in order to more accurately model the LHC Higgs signal. The resummation for the zero-jet bin cross section in the presence of the anti-k_T algorithm was first obtained at next-to-leading logarithmic (NLL) accuracy [30] and later extended to NNLL accuracy [35, 36] using two different theoretical approaches. The importance of potentially large $\ln R$ corrections on numerical predictions, where R is the jet-radius parameter in the anti-k_T algorithm, was studied in Ref. [37]. A significant reduction of the residual theoretical uncertainties was obtained in the zero-jet bin by resumming the jet-veto logarithms. Given that the theoretical uncertainties are currently one of the largest systematic errors affecting the one-jet bin analyses of the Higgs-like particle properties [38], it is desirable to formulate the resummation when final-state jets are also present.

In a previous paper we established the formalism necessary for resummation of the Higgs plus jet process by deriving a factorization theorem using soft-collinear effective theory (SCET) [39–43] for the production of color-neutral particle and one or more jets in the presence of a jet-veto [44]. This result assumes that the transverse momenta of all hard jets are larger than the veto scale. We calculated contributions through next-to-leading order in the exponent of the Sudakov form factor, and presented initial numerical results for Higgs production in association with a jet at the LHC. We found that resummation of the jet-veto logarithms significantly improves the reliability of the perturbative expansion, and could potentially lead to a reduced theoretical systematic error in experimental studies.

In this manuscript we extend the calculation of Ref. [44] in several ways. We first present a calculation of the NLO soft function appearing in the factorization theorem for exclusive

Higgs plus one-jet production. This allows the extension of the resummation accuracy to NLL$'$ accuracy, using the logarithmic counting established in Ref. [33]. This level of logarithmic accuracy implies that we correctly obtain the first three logarithmic corrections at each order in the QCD coupling constant: $\alpha_s L^2$, $\alpha_s L$ and α_s; $\alpha_s^2 L^4$, $\alpha_s^2 L^3$, and $\alpha_s^2 L^2$; $\alpha_s^3 L^6$, $\alpha_s^3 L^5$, $\alpha_s^3 L^4$; and so on. We match our results to fixed-order to obtain a NLL$' +$ NLO prediction, and present numerical results for use in LHC analyses. We first demonstrate that the region of phase space where the leading-jet transverse momentum is of order the Higgs mass accounts for nearly half of the error in the fixed-order NLO prediction for Higgs plus one jet, and is therefore a prime candidate for an improved theoretical treatment. We then perform a detailed study of the residual theoretical uncertainties using our resummed prediction that accounts for the variation of all unphysical scales remaining in the prediction. Even with a very conservative treatment of the errors, a significant reduction of the residual uncertainty as compared to the fixed-order estimate is found; the estimated uncertainties decrease by up to a quarter of their initial values. Our results, and the improvements in the zero-jet bin obtained previously, should form the basis for future theoretical error estimates in experimental analyses of Higgs properties.

Our paper is organized as follows. We review the factorization theorem of Ref. [44] in Section II. We discuss the extension of the resummation to the NLL$'$ level in Section III, and present the calculation of the previously unknown one-loop soft function. A detailed discussion of numerical results for the LHC is given in Section IV. We describe there how we estimate theoretical uncertainties in both the fixed-order and resummed results, and demonstrate that the resummation of jet-veto logarithms reduces the theoretical systematic error affecting LHC analyses. Finally, we conclude in Section V. Many technical details needed for the numerical studies are given in the Appendix.

II. REVIEW OF THE FACTORIZATION THEOREM

We begin by reviewing the salient features of the factorization theorem for exclusive Higgs plus one-jet production [44]. The factorization of the cross section into separate hard, soft, and collinear sectors is complicated by the presence of the jet algorithm needed to obtain an infrared-safe observable. Following the experimental analyses, we use the anti-k_T

algorithm [45] to define jets. Anti-k_T jets are built using the following distance metrics:

$$\begin{aligned} \rho_{ij} &= \min(p_{T,i}^{-1}, p_{T,j}^{-1})\Delta R_{ij}/R, \\ \rho_i &= p_{T,i}^{-1}. \end{aligned} \tag{1}$$

The anti-k_T algorithm merges particles i and j to form a new particle by adding their four-momenta if ρ_{ij} is the smallest among all the metrics. Otherwise, i or j is promoted to a jet depending on whether ρ_i or ρ_j is smaller, and removed from the set of considered particles. This procedure is repeated until all particles are grouped into jets. We note that $\Delta R_{ij}^2 = \Delta\eta_{ij}^2 + \Delta\phi_{ij}^2$, where $\Delta\eta_{ij}$ and $\Delta\phi_{ij}$ are the rapidity and azimuthal angle difference between particles i and j, respectively. R is the jet-radius parameter, which in practice is chosen to be around $0.4 - 0.5$.

We demand that the final state contain only a single jet with $p_T^J > p_T^{veto} \sim 25 - 30$ GeV. Other jets with a transverse momentum above this threshold are vetoed. Since p_T^{veto} is usually substantially lower than the partonic center-of-mass energy ($\lambda \equiv p_T^{veto}/\sqrt{\hat{s}} \ll 1$), the vetoed observables are usually very sensitive to soft and collinear emissions. We will make the following assumptions in order to proceed in our analysis:

$$p_T^J \sim m_H \sim \sqrt{\hat{s}}; \quad 1 \gg R^2 \gg \lambda^2; \quad \frac{\alpha_s}{2\pi}\log^2 R \ll 1. \tag{2}$$

The first assumption leaves us with a two-scale problem and allows the measured final-state jet to be described by a separate collinear sector. The second of these requirements is necessary to insure that the measurement function factorizes into separate measurements in each of the collinear sectors. The third requirement ensures that logarithms associated with the anti-k_T parameter R need not be resummed. We will see later that the first assumption is satisfied in approximately 30% of the relevant phase space for Higgs plus jet production at the LHC, and that this parameter region contributes roughly half of the total error. We will therefore be able to improve the theoretical description of a significant fraction of the LHC Higgs signal. Given that $p_T^{veto} \approx 25 - 30\,\text{GeV}$ and $R \approx 0.4 - 0.5$, when the leading jet $p_T^J \sim m_H$, the second two assumptions are also justified.

Our effective theory consists of the following low-energy degrees of freedom:

- a collinear jet mode with momentum $p_J = \frac{\omega_J}{2} n_J + k_J$, where n_J is the light-cone vector along the jet direction;

- two collinear modes propagating along the beam axes a and b, with $p_i = \frac{\omega_i}{2} n_i + k_i$ for $i = a, b$;

- a soft mode with momentum k_s.

The residual momenta k_J, k_i and the soft momentum k_s all scale as $\sqrt{\hat{s}}\lambda$, while the large components of the three collinear momenta scale as $\omega_i \sim \sqrt{\hat{s}}$. Momenta with smaller scalings, such as ultrasoft modes, do not contribute to the final-state observable and can be integrated over, and therefore need not be introduced. We are able to utilize an effective-theory framework because of how the anti-k_T algorithm clusters the soft and collinear modes. Referring to the metrics defined in Eq. (1), we find

$$\begin{aligned}
&\rho_{JJ} \lesssim \rho_J \sim 1\,, \quad \rho_{Js} \sim R^{-1}\,, \quad \rho_{Ja} \sim \rho_{Jb} \sim R^{-1} \log \lambda^{-1}\,, \\
&\rho_{ss} \sim \rho_{aa} \sim \rho_{bb} \sim (\lambda R)^{-1}\,, \quad \rho_{sa} \sim \rho_{sb} \sim \rho_{ab} \sim (\lambda R)^{-1} \log \lambda^{-1}\,, \\
&\rho_s \sim \rho_a \sim \rho_b \sim \lambda^{-1}\,.
\end{aligned} \tag{3}$$

From ρ_{JJ} and ρ_J in the first line, we see that the initial clustering combines the final-state hard emissions into a jet, so that the soft radiation sees only the jet direction and does not probe its internal structure. Also, since the clustering between the soft and jet radiation typically occurs earlier than the clustering among the soft radiation, clustering of soft particles across the jet boundary is unlikely to happen [45, 46]. We see from the second line that the mixing between the soft and beam sectors is power-suppressed, as is the mixing between the beam and jet sectors. Denoting the measurement function that imposes the jet clustering and vetoing as $\hat{\mathcal{M}}$, these factors imply that we can factor $\hat{\mathcal{M}}$ into the product of measurement functions acting separately on the soft, jet, and beam sectors,

$$\hat{\mathcal{M}} = \hat{\mathcal{M}}_J \hat{\mathcal{M}}_s \hat{\mathcal{M}}_a \hat{\mathcal{M}}_b, \tag{4}$$

up to power-suppressed corrections in p_T^{veto} and R.

The remaining steps in the derivation of the factorization theorem utilize the standard SCET machinery, and are presented in detail in Ref. [44]. The final result for the cross section for exclusive Higgs plus one-jet production takes the following form:

$$\begin{aligned}
\mathrm{d}\sigma_{\mathrm{NLL}'} \;=\; & \mathrm{d}\Phi_H \mathrm{d}\Phi_J\, \mathcal{F}(\Phi_H, \Phi_J) \sum_{a,b} \int \mathrm{d}x_a \mathrm{d}x_b \frac{1}{2\hat{s}}\, (2\pi)^4 \delta^4\left(q_a + q_b - q_J - q_H\right) \\
& \times \sum_{\text{spin}}^{-} \sum_{\text{color}}^{-} \mathrm{Tr}(H \cdot S)\, \mathcal{I}_{a,i_a j_a} \otimes f_{j_a}(x_a)\, \mathcal{I}_{b,i_b j_b} \otimes f_{j_b}(x_b) J_J(R)\,.
\end{aligned} \tag{5}$$

We have denoted explicitly by the subscript that we will evaluate this cross section to the NLL$'$ level. $\mathrm{d}\Phi_H$ and $\mathrm{d}\Phi_{j_i}$ are the phase space measures for the Higgs and the massless jet J, respectively. $\mathcal{F}(\Phi_{H_c}, \Phi_J)$ includes all additional phase-space cuts other than the p_T veto acting on the Higgs boson and the hard jet. H is the hard function that comes from matching full QCD onto SCET, and S describes soft final-state emissions. The trace is over the color indices. The functions $\mathcal{I}$ and J describe collinear emissions along the beam axes and along the final-state jet direction, respectively. The measured jet p_T^J should be much larger than p_T^{veto}. Operator definitions for all functions are given in Ref. [44]. As our purpose here is to only briefly review the factorization theorem before presenting new results, we do not reproduce these definitions explicitly, and instead refer the reader to the quoted reference. The tree-level and one-loop expressions for the jet and beam functions needed for numerical studies are presented in the Appendix.

III. EXTENSION TO NLL$'$

A primary goal of this manuscript is to extend the resummation of jet-veto logarithms to the NLL$'$ level, following the notation of Ref. [33]. This level of logarithmic accuracy implies that we correctly obtain the following towers of logarithms: $\alpha_s L^2$, $\alpha_s L$ and α_s; $\alpha_s^2 L^4$, $\alpha_s^2 L^3$, and $\alpha_s^2 L^2$; $\alpha_s^3 L^6$, $\alpha_s^3 L^5$, $\alpha_s^3 L^4$; and so on. The following ingredients are required to obtain this accuracy:

- the two-loop cusp and one-loop non-cusp anomalous dimensions which control the evolution of the beam, jet, soft and hard functions;
- the one-loop hard, beam and jet functions;
- the one-loop soft function.

The requisite anomalous dimensions, as well as the one-loop jet and beam functions, were obtained in Ref. [44]. They are included in the Appendix for completeness, as is a detailed discussion of their implementation into Eq. (5). The one-loop hard function for the gg, qg and $q\bar{q}$ channels can be obtained from the literature [47]. The previously unknown quantity is the one-loop soft function. Its calculation is rendered non-trivial by the presence of the final-state jet. We describe our computation of the soft function below.

A. Calculation of the one-loop soft function

We begin by defining the measurement function for the soft sector:

$$\hat{\mathcal{M}}_s = \Theta_{p_T^{veto},k_T}\Theta_{\Delta R_{kJ},R} + \Theta_{R,\Delta R_{kJ}}, \tag{6}$$

where we have set $\Theta_{a,b} = \theta(a-b)$ and $\Delta R_{kJ} = \sqrt{\Delta y^2 + \Delta\phi^2}$. The first term allows soft emissions that are well-separated from the final-state jet but have a transverse momentum softer than p_T^{veto}, while the second term allows harder emissions that are within the final-state jet radius. As the soft function is simply the square of the soft current integrated over the allowed phase space, we can immediately write the NLO contribution to the soft function as

$$S = -\frac{2g_s^2}{(2\pi)^{d-1}}\sum_{i<j} T_i\cdot T_j \int \mathrm{d}^d k\,\delta(k^2)\frac{n_i\cdot n_j}{n_i\cdot k n_j\cdot k}\,\hat{\mathcal{M}}_s, \tag{7}$$

where the sum is over the two beam directions and the final-state jet direction. The n_i denote light-like vectors in each of these directions, while the T_i denote color operators in either the fundamental or adjoint representations, depending on whether i denotes a quark or a gluon. k is the momentum of the gluon emitted from the eikonal lines. We note that the leading-order soft function is normalized to unity. Parameterizing

$$\begin{aligned} k^\mu &= k_T\left(\cosh y, \cos\phi, \sin\phi, \sinh y\right), \\ n_J^\mu &= (\cosh y_J, 1, 0, \sinh y_J), \end{aligned} \tag{8}$$

and setting

$$\Theta_{\Delta R_{kJ},R} = 1 - \Theta_{R,\Delta R_{kJ}}\,, \tag{9}$$

we find

$$\begin{aligned} S &= -g_s^2\frac{\Omega_{1-2\epsilon}}{2(2\pi)^{d-1}}\sum_{i<j} T_i\cdot T_j \int \mathrm{d}y\,\mathrm{d}\phi\,\mathrm{d}k_T^2\,(s_\phi)^{-2\epsilon}\,(k_T^2)^{-\epsilon}\frac{n_i\cdot n_j}{n_i\cdot k n_j\cdot k} \\ &\times \left(\Theta_{p_T^{veto},k_T} + \Theta_{R,\Delta R_{kJ}}\Theta_{k_T,p_T^{veto}}\right) \end{aligned} \tag{10}$$

where Ω_d denotes the d-dimensional solid angle and $s_\phi = \sin\phi$.

We will proceed by reducing these integrals as far as possible analytically, although we will end up with two remaining integrals which we evaluate numerically. Since the first

such integral is a pure number, while the second depends only upon R, this does not affect the speed of the numerical program we construct. We note that the soft function will have rapidity divergences arising from the $n_i \cdot k$ in the denominator of Eq. (10), which we will regulate by multiplying the integrand by the following factor [49]:

$$|2k_{g,3}|^{-\eta}\nu^{\eta}. \tag{11}$$

This regulates the rapidity divergence as a pole in η, which is then removed by renormalization. There are two distinct structures to consider in Eq. (10): the first when both i and j denote a beam direction, and the second when i denotes the jet direction. We write the soft function as

$$S = T_a \cdot T_b \, S_{n\bar{n}} + T_a \cdot T_J \, S_{nJ} + T_b \cdot T_J \, S_{\bar{n}J} \tag{12}$$

and study each structure separately. We note before continuing that the virtual corrections are scaleless, and have the effect of converting the infrared poles in the real-emission corrections into ultraviolet poles.

$\underline{S_{n\bar{n}}}$: This case will have rapidity divergences as $n \cdot k \to 0$ and $\bar{n} \cdot k \to 0$. We can therefore replace the regulator of Eq. (11) using

$$|2k_{g,3}|^{-\eta}\nu^{\eta} \xrightarrow{|y|\to\infty} k_T^{-\eta}\nu^{\eta}\exp(-\eta\,|y|)\,. \tag{13}$$

This relation is valid in the large y limit in which the rapidity divergence occurs. Since we are treating $\mathcal{O}(R)$ contributions as power-suppressed terms and there are no singularities associated with emissions along the final-state jet direction, we can expand $\Theta_{\Delta R_{kJ},R} = 1 + \mathcal{O}(R)$ to derive

$$S_{n\bar{n}} = g_s^2 \frac{2\Omega_{2-2\epsilon}}{(2\pi)^{d-1}} \frac{1}{2\epsilon+\eta} \left(\frac{p_T^{veto}}{\mu}\right)^{-2\epsilon-\eta} \left(\frac{\nu}{\mu}\right)^{\eta} \frac{2}{\eta}. \tag{14}$$

This can be easily expanded in both η and ϵ in order to isolate the poles, which are then removed by renormalization.

$\underline{S_{nn_J}}$: The calculation of this structure is more involved than the previous one. We first note that the $n \cdot k \to 0$ rapidity divergence is correctly regulated by the following replacement, valid in the large-y limit in which the divergence occurs:

$$|2k_{g,3}|^{-\eta}\nu^{\eta} = 2^{-\eta}k_T^{-\eta}\nu^{\eta}|\sinh y|^{-\eta} \xrightarrow{y\to\infty} k_T^{-\eta}\nu^{\eta}\exp(-\eta\, y\,\Theta(y))\,. \tag{15}$$

Performing the k_T integration in Eq. (10), and afterwards using the relation $\Theta_{\Delta R_{kJ},R} = 1 - \Theta_{R,\Delta R_{kJ}}$, we find

$$\begin{aligned} S_{nn_J} &= g_S^2 \frac{\Omega_{1-2\epsilon}}{(2\pi)^{d-1}} \frac{\pi}{2\epsilon+\eta} \left(\frac{p_T^{veto}}{\mu}\right)^{-2\epsilon-\eta} \left(\frac{\nu \exp(-y_J)}{\mu}\right)^{\eta} \\ &\quad \times \int_{-\infty}^{\infty} \mathrm{d}\Delta y \int_0^{\pi} \frac{\mathrm{d}\phi}{\pi} (s_\phi)^{-2\epsilon} \frac{\exp(\Delta y)\exp(-\eta \Delta y\, \Theta(\Delta y))}{(\cosh \Delta y - \cos\phi)} \Theta_{\Delta R_{kJ},R}\,, \end{aligned} \tag{16}$$

where we have shifted the integration variables to $\Delta y = y - y_J$. We can no longer directly expand the integrand for $R \to 0$, as there is a logarithmic divergence in this limit associated with collinear emissions along the final-state jet direction. We will proceed by isolating the small-R behavior of the integrand by defining

$$\begin{aligned} \mathcal{I} &\equiv (s_\phi)^{-2\epsilon} \frac{\exp(\Delta y)\exp(-\eta \Delta y\, \Theta(\Delta y))}{(\cosh \Delta y - \cos\phi)}\,, \\ \mathcal{I}_R &\equiv (s_\phi)^{-2\epsilon} \frac{2\, \exp(-\eta \Delta y\, \Theta(\Delta y))}{(\Delta y^2 + \phi^2)}\,. \end{aligned} \tag{17}$$

We divide the integrand into the two structure $\mathcal{I} - \mathcal{I}_R$ and $\mathcal{I}_R$. The first piece is finite as $R \to 0$ and can be Taylor-expanded in that limit, while the second contains $\ln R$ behavior and cannot. We further find it convenient for the $\mathcal{I} - \mathcal{I}_R$ term to divide the Δy integral into two regions: $\Delta y < 0$, for which the rapidity divergence cannot occur and consequently we can set $\eta = 0$; $\Delta y > 0$, in which the rapidity divergence can occur and η must be retained. Performing the indicated manipulations, we reduce S_{nn_J} into the sum of three structures:

$$S_{nn_J} = S_{nn_J}^{\ln R} + S_{nn_J}^{\eta} + S_{nn_J}^{\eta=0}, \tag{18}$$

where we have identified

$$\begin{aligned} S_{nn_J}^{\ln R} &= g_s^2 \frac{\Omega_{1-2\epsilon}}{(2\pi)^{d-1}} \frac{\pi}{2\epsilon} \left(\frac{p_T^{veto}}{\mu}\right)^{-2\epsilon} \int_{-\infty}^{\infty} \mathrm{d}\Delta y \int_0^{\pi} \frac{\mathrm{d}\Delta\phi}{\pi} (s_{\Delta\phi})^{-2\epsilon} \frac{2}{{\Delta R_{kJ}}^2} \Theta_{\Delta R_{kJ},R}\,, \\ S_{nn_J}^{\eta} &= g_s^2 \frac{\Omega_{2-2\epsilon}}{(2\pi)^{d-1}} \frac{1}{2\epsilon+\eta} \left(\frac{p_T^{veto}}{\mu}\right)^{-2\epsilon-\eta} \left(\frac{\nu \exp(-y_J)}{\mu}\right)^{\eta} \frac{2}{\eta}\,, \\ S_{nn_J}^{\eta=0} &= g_s^2 \frac{\Omega_{1-2\epsilon}}{(2\pi)^{d-1}} \frac{\pi}{2\epsilon} \left(\frac{p_T^{veto}}{\mu}\right)^{-2\epsilon} \int_{-\infty}^{\infty} \mathrm{d}\Delta y \int_0^{\pi} \frac{\mathrm{d}\Delta\phi}{\pi} \left[\mathcal{I} - \mathcal{I}_R - 2(s_{\Delta\phi})^{-2\epsilon}\Theta(\Delta y)\right]\,. \end{aligned} \tag{19}$$

We will numerically calculate the integrals which are left upon expansion of the integrands in ϵ. We note that the $S_{\bar{n}n_J}$ term of Eq. (12) can be obtained by taking $y_J \to -y_J$ in Eq. (19), which affects only the $S_{nn_J}^{\eta}$ structure above.

Combining all of the information presented above, expanding in both η and ϵ and removing the poles via renormalization, we are left with the following final result for the soft

function:

$$S = \frac{\alpha_s}{4\pi}\left\{(T_a^2+T_b^2)\left[L^2+4\ln\frac{p_T^{veto}}{\nu}L\right]+2\,T_J^2\,L\ln R^2+4\,y_J\,L\,(T_a\cdot T_J-T_b\cdot T_J)\right.$$
$$\left.-\;(T_a^2+T_b^2)\frac{\pi^2}{6}+T_J^2\,[c+f(R)]\right., \tag{20}$$

where we have abbreviated $L=\ln(\mu^2/p_T^{veto,2})$. The constant c and function $f(R)$ are given by the following integrals:

$$c = 4\int_{-\infty}^{\infty}\mathrm{d}\Delta y\int_0^{\pi}\frac{\mathrm{d}\phi}{\pi}\left(\mathcal{I}^{\eta=0,\epsilon=0}-\mathcal{I}_R^{\eta=0,\epsilon=0}-2\Theta(\Delta y)\right)\log(s_\phi)\,,$$
$$f(R) = -4\log(2)\log R^2+8\int_{-\infty}^{\infty}\mathrm{d}\Delta y\int_0^{\pi}\frac{\mathrm{d}\phi}{\pi}\frac{\log(s_\phi)}{{\Delta R_{kJ}}^2}\,\Theta_{\Delta R_{kJ},R}\,. \tag{21}$$

As stated above, we determine these quantities numerically in our analysis. As we only perform our analysis for a very small set of R values, this is sufficient for our purposes. We note that the L^2 and L terms agree with those predicted in Ref. [44] using the cancellation of the combined running of the hard, jet, beam and soft functions. For the Higgs production process considered in this work, we have the following color identities: for the ggg channel, $T_i\cdot T_j=-C_A/2$; for the $q_1\bar{q}_2g_3$ channel, $T_1\cdot T_2=-(C_F-C_A/2)$ and $T_1\cdot T_3=T_2\cdot T_3=-C_A/2$.

IV. NUMERICAL RESULTS

We now present numerical results for exclusive Higgs plus one-jet production at the LHC. We first discuss the matching of the resummed result with the NLO cross section to obtain a renormalization-group (RG) improved NLL$'$ + NLO prediction, and demonstrate that we correctly capture the large logarithms associated with p_T^{veto}. We also discuss the parameter region in which our effective-theory framework is valid. Although this region, with $p_T^J\sim m_H$, makes up only ∼25-30% of the signal, it accounts for nearly half of the theoretical uncertainty in the one-jet bin. We then describe in detail how we estimate the theoretical uncertainties in both the fixed-order and RG-improved results. For the fixed-order cross section we follow the "ST" recommendations of Ref. [32]. Our treatment of the theoretical uncertainties of the RG-improved result is necessarily more involved, as our effective-theory approach improves the prediction over only part of the relevant phase space. We adopt a combination of direct scale variation, which is standard in resummed calculation [32], and the ST recommendations for the fixed-order region, as described below. Finally, we show

that the resummation of the jet-veto logarithms leads to a sizable reduction of the exclusive Higgs plus one-jet uncertainties at the LHC.

A. Matching NLL′ with NLO

We begin by matching our resummed expression with the fixed-order NLO result to obtain a NLL′ + NLO prediction. We use the NLO predictions for Higgs plus one-jet contained in MCFM [50]. We obtain our prediction by setting

$$\sigma_{\text{NLL}'+\text{NLO}} = \sigma_{\text{NLL}'} + \sigma_{\text{NLO}} - \sigma^{\text{exp}}_{\text{NLL}'}. \tag{22}$$

In this equation, σ_{NLO} is the fixed-order NLO cross section obtained from MCFM, and σ'_{NLL} is the resummed cross section up to NLL′ accuracy presented in Eq. (5). $\sigma^{\text{exp}}_{\text{NLL}'}$ captures the singular features of σ_{NLO}, and is obtained by expanding $\sigma_{\text{NLL}'}$ with all scales set to a common value μ. Schematically, we have

$$\begin{aligned}
\sigma_{\text{NLL}'} &= \sigma_{\text{LO}} \left(1 + \alpha_s g_0\right) e^{-L g_{\text{LL}}(\alpha_s L) - g_{\text{NLL}}(\alpha_s L)} \\
\sigma^{\text{exp}}_{\text{NLL}'} &= \sigma_{\text{LO}} \left(1 + \alpha_s \left[-g_2 L^2 - g_1 L + g_0\right]\right) ,
\end{aligned} \tag{23}$$

where $L\, g_{\text{LL}}$ and g_{NLL} resum the leading and next-to-leading logarithms, respectively. The difference between σ_{NLO} and the expanded NLL' result $\sigma^{\text{exp}}_{\text{NLL}'}$ only contains power-suppressed contributions for large values of Q:

$$\sigma_{\text{non-singular}} \equiv \sigma_{\text{NLO}} - \sigma^{\text{exp}}_{\text{NLL}'} \sim \mathcal{O}\left(R^2 L, \frac{p_T^{veto}}{Q} L\,, \frac{p_T^{veto}}{Q} \log R\,, \cdots\right) , \tag{24}$$

with $L = \log\left(Q/p_T^{veto}\right)$, and Q stands for any kinematic quantity of order m_H. Since the scale QR is used to define the jet mode, the $R^2 L$ terms are regarded as power suppressed.

To demonstrate that our formalism correctly captures the singular terms at NLO as $L \to 0$, we plot in Fig. 1 the fractional difference between the expanded cross section $\sigma^{\text{exp}}_{\text{NLL}'}$ and the NLO result as a function of p_T^{veto}. We note that due to the power-suppressed $R^n L$ terms, the difference does not completely vanish as p_T^{veto} goes to 0 for fixed R. However, we see from the several R values plotted in Fig. 1 that in the $R \to 0$ limit, these terms also vanish, as expected.

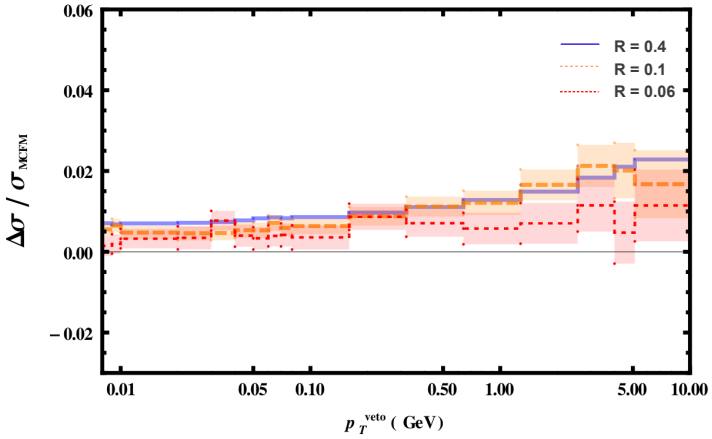

FIG. 1: Shown are the fractional differences $(\sigma_{\rm NLO} - \sigma^{\rm exp}_{\rm NLL'})/\sigma_{\rm NLO}$ for $R = 0.4$ (solid blue), 0.1(dashed orange) and 0.06 (dotted red), respectively. The colored bands represent the estimated numerical uncertainties. The differences between the expanded NLL′ and the fixed-order NLO calculations are small compared with the total cross section.

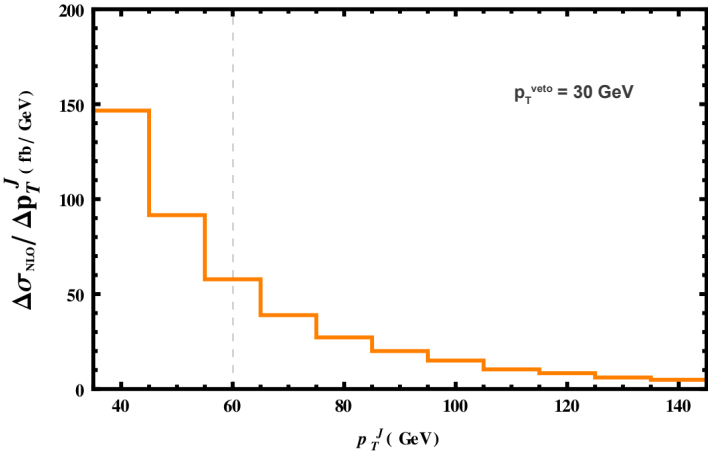

FIG. 2: $\Delta\sigma/\Delta p_T^J$ is the bin-integrated cross section for Higgs plus one jet as a function of p_T^J divided by the bin width. We assume $p_T^{veto} = 30\,\text{GeV}$. If we define the lower boundary of the $p_T^J \sim \mathcal{O}(m_H)$ region by $p_T^J = m_H/2$, we can estimate the contribution from $p_T^J \sim \mathcal{O}(m_H)$ to be around 30%.

B. Validity of the effective theory

Having demonstrated that our NLL′ result correctly captures the logarithms of p_T^{veto}, we comment here briefly on its expected range of validity. In our derivation of the factorization theorem, we assumed that the signal jet p_T^J is of order m_H. From Fig. 2, we see that this configuration contributes a non-negligible fraction of the experimentally-interesting total cross section for $p_T^{veto} \sim 30$ GeV and $p_T^J > p_T^{veto}$. Our factorization theorem holds for $p_T^{veto} \ll p_T^J \sim Q$, but breaks down when $p_T^J \sim p_T^{veto} \ll m_H$. Additional large logarithms of the form $\ln^2 m_H/p_T^J$ and $L \times p_T^{veto}/p_T^J$ are not resummed in our formalism. We describe these terms only as well as a fixed-order NLO calculation. A different effective theory is needed for this regime to correctly sum the large logarithms. We do not consider this theory in this manuscript; our goal here is to consistently apply the currently available formalism at NLL′ + NLO to see to what extent we can reduce the theoretical uncertainty.

Interestingly, the $p_T^J \sim m_H$ region contributes roughly 50% of the uncertainty in the one-jet bin, larger than might be expected from Fig. 2. We show this by computing the NLO cross section for an example parameter choice. We set $m_H = 126$ GeV and $p_T^{veto} = 25$ GeV, and divide the Higgs plus one-jet cross section, whose inclusive value is $\sigma^{1j}_{\rm NLO} = 5.75^{+2.03}_{-2.66}\,\text{pb}$, into two bins: the first with $p_T^J < m_H/2$, and the second with $p_T^J > m_H/2$. As explained in detail later in Sec. IV C, we use the fixed-order cross section in the first bin since our effective-theory analysis does not hold, and turn on resummation in the second bin. Computing the cross section at NLO in each bin, and estimating the uncertainties as described in detail in Sec. IV C, we find

$$\begin{aligned} \sigma^{1j}_{\rm NLO}(p_T^J < m_H/2) &= 4.74^{+1.31}_{-1.29}\,\text{pb}, \\ \sigma^{1j}_{\rm NLO}(p_T^J > m_H/2) &= 1.01^{+0.85}_{-1.51}\,\text{pb}. \end{aligned} \tag{25}$$

The central values have been obtained using the scale choice for $\mu = m_H/2$.[1] Although it accounts for less than 25% of the cross section, the region where our effective-theory analysis can improve the uncertainties contributes roughly half of the error in the full one-jet bin.

We briefly comment here on non-global logarithms [48] that first occur at the NLL′ level. Although they are not included in our current factorization theorem, to estimate their

[1] We note that using a larger central scale choice leads to the same conclusions regarding the relative uncertainties of the two bins.

numerical effect we use the large-N_c resummation of these terms derived in Ref. [48]. We include them as a multiplicative correction to our factorization formula. Their numerical effect is small, at or below one percent of the total exclusive Higgs plus one-jet production rate for the relevant values of m_H and p_T^{veto}. To check the robustness of this result we vary the hard scale appearing in these corrections by a factor of two around their nominal value of m_H, and find similarly small corrections. We therefore believe that it is numerically safe to neglect these terms in our NLL$'$ result, although they should be further investigated in the future.

C. Scale choices and uncertainty estimation

Since the resummation holds only for $p_T \sim m_H$, we wish to turn it off and recover the fixed-order NLO result as p_T^J becomes small. To do so, we note that the fixed order cross section $\sigma_{\rm NLO}$ and the expanded NLL$'$ cross section $\sigma^{\rm exp}_{\rm NLL'}$ depend only on the scale $\mu_R = \mu_F = \mu$, while $\sigma_{\rm NLL'}$ also depends on the scales μ_H, μ_J, μ_B, μ_S, ν_B and ν_S that appear in the hard, jet, beam and soft functions. The optimal choice for each scale can be determined by minimizing the higher order corrections to each separate component. These functions are then RG-evolved to the common scale μ. Consequently, the resummation can be turned off by setting all scales to μ , so that the full NLL$'$ + NLO result reduces to the NLO one. We adopt a conservative scheme to turn off the resummation as soon as possible, as suggested in Ref. [33]. In the region where $p_T^J \gg p_T^{veto}$, we keep the resummation on. When $p_T^J \sim p_T^{veto}$, we switch off the resummation by setting all scales to μ, which leads to the fixed-order prediction. We interpolate between these two regions smoothly using

$$\mu_i^{int.} = \mu + (\mu_i - \mu)\left[\,1 + \tanh\left(\kappa\left(p_T^J - p_{\rm off}\right)\right)\,\right]/2\,, \tag{26}$$

where the index i runs over all appearing scales. We use similar expressions for the ν's. Our numerical predictions are obtained using the $\mu_i^{int.}$ expressions in our code. When $p_T^J < p_{\rm off}$, the resummation starts to vanish. We set $p_{\rm off} = \max(2p_T^{veto}, \frac{m_H}{2})$ to be the default value.[2] The slope κ controls how smoothly we turn off the resummation. We find that

[2] The reason for this choice is that our EFT is valid when p_T^J is located in the hard domain whose lower boundary is estimated to be $\frac{m_H}{2}$, and it entirely breaks down when p_T^J falls into the "soft" regime whose upper boundary is roughly $2p_T^{veto}$.

the interpolated cross section is insensitive to the choice of κ. The functional forms of the interpolation in Eq. (26) for various values κ are shown in Fig. 3. When making uncertainty estimations, we vary each scale separately. In the resummation region, the cross section is relatively insensitive to the variation of μ. In the fixed-order range, it is insensitive to μ_i and ν_i.

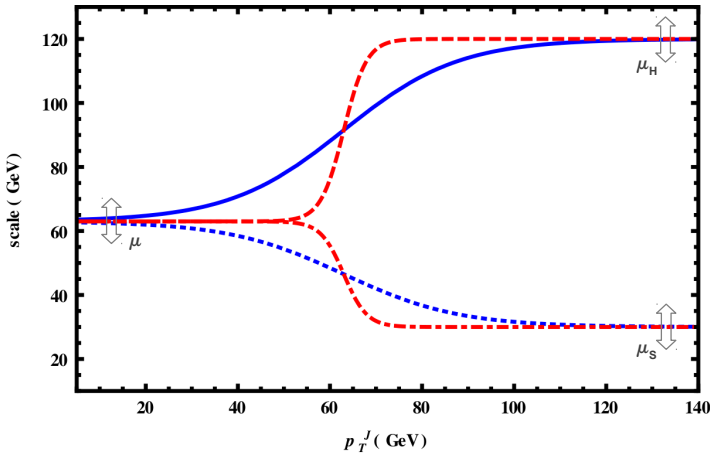

FIG. 3: Shown is the interpolation between the resummed result and the fixed-order one proposed in Eq. (26). The blue solid and dotted lines are for $\kappa = 0.04$ and the red dashed and dot-dashed lines are for $\kappa = 0.2$. When p_T^J is less than $p_{\rm off}$, all the scales merge to μ and the cross section takes its NLO value. We have demonstrated this behavior for the hard and soft scales in the plot.

We describe here in detail how we estimate the uncertainties in both the fixed-order and RG-improved results. We vary all scales appearing in the cross section around their central values by factors of two in both directions in order to estimate the theoretical error. To avoid an underestimate of the uncertainty of the fixed-order calculation, we follow the procedure suggested by Stewart and Tackmann [32]. We split the exclusive one-jet cross section into the difference of one-jet inclusive and two-jet inclusive results:

$$\sigma_{1j} = \sigma_{\geq 1j} - \sigma_{\geq 2j} \,. \tag{27}$$

We estimate the scale uncertainty for each piece separately and add them in quadrature to obtain the scale uncertainty for the exclusive cross section:

$$\delta^2_{1j,\rm NLO} = \delta^2_{\geq 1j,\rm NLO} + \delta^2_{\geq 2j,\rm NLO} \,. \tag{28}$$

For the NLL$'$ + NLO result, the uncertainty is derived by adding in quadrature the separate variations of all scales which enter [32]:

$$\delta_{1j}^2 = \delta^2_{\rm non-singular,\mu} + \delta^2_{\rm NLL',\mu} + \delta^2_{\rm NLL',\mu_H} + \delta^2_{\rm NLL',\mu_J} + \delta^2_{\rm NLL',\mu_B,\nu_B} + \delta^2_{\rm NLL',\mu_S,\nu_S}\,. \qquad (29)$$

Before continuing we comment briefly on the structure of Eq. (29). In order to perform the matching to fixed order in Eq. (22), we RG-evolve the NLL$'$ result so that all scales are set to the common scale μ. We then add on the non-singular NLO terms via the difference between the full NLO cross section and the expanded NLL$'$ results. This explains the first two contributions to the above equations. As the hard and jet functions live at the scales $\sqrt{m_H p_T^J}$ and $p_T^J R$ respectively [44], these scale variations are treated as uncorrelated in Eq. (29). Finally, the variations of beam and soft functions, which live at the scale p_T^{veto}, are added to this.

When we apply this formalism and assume actual LHC kinematic cuts, a large fraction of the cross section comes from the low-p_T^J regime where $p_T^J < p_{\rm off}$, and the fixed-order calculation dominates. In this situation, we split the cross section into two regions, one with $p_T^{veto} < p_T^J < p_{\rm off}$ and the other with $p_T^J > p_{\rm off}$. For the former region, we use Eq. (28) to estimate the uncertainty and for the latter one, we utilize Eq. (29). We combine these two linearly to estimate the scale dependence for the RG-improved cross section:

$$\delta_{1j}(p_T^J > p_T^{veto}) = \delta_{1j,\rm NLO}(p_T^J < p_{\rm off}) + \delta_{1j}(p_T^J > p_{\rm off})\,. \qquad (30)$$

Since the resummation in the result used for $p_T^J > p_{\rm off}$ is turned off quickly by using the interpolation in Eq. (26), and the uncertainty of the fixed-order cross section used for $p_T^J < p_{\rm off}$ is obtained using the ST prescription, we believe that this leads to a very conservative estimate of the theoretical error after performing our RG-improvement.

D. Numerics for the LHC

We now present predictions and uncertainty estimates for use in LHC analyses. For the following numerical results, and those shown above, we use the MSTW 2008 parton distribution functions [51] at NLO. We assume an 8 TeV LHC, and $m_H = 126$ GeV unless stated otherwise. We demand that the leading jet be produced with rapidity $|y_J| < 4.5$, and veto all other jets with $p_T > p_T^{veto}$ over the entire rapidity range. The following central

values are used for the scales which appear:

$$\begin{aligned}
&\mu = \sqrt{(m_H^T)_{\min}(p_T^J)_{\min}}, \qquad \mu_H = \sqrt{m_H^T p_T^J}\,, \\
&\mu_J = p_T^J R\,, \qquad \mu_B = \mu_S = p_T^{veto}\,, \\
&\nu_{B_{a,b}} = x_{a,b}\sqrt{s}\,, \qquad \nu_S = p_T^{veto}\,.
\end{aligned} \tag{31}$$

where $m_H^T = \sqrt{m_H^2 + p_T^{J,2}}$. We note that these central scale values, as well as the variations up and down by a factor of two, are used as the μ_i on the right-hand side of Eq. (26). The actual numerical scale choices used in the code are the $\mu_i^{int.}$ appearing on the left-hand side of Eq. (26). We use $\kappa = 0.2$ to produce all numerical results, although we have checked that their dependence on κ is negligible.

We begin by showing in Fig. 4 the NLO and NLL$'$ + NLO results for $p_T^J > 120$ GeV as a function of p_T^{veto}, to make clear the improvement gained by adding the resummation in the $p_T^J \sim m_H$ region. After resummation, the scale dependence has been dramatically reduced for small p_T^{veto}. For large p_T^{veto} the RG-improved cross section tends toward the fixed-order result, as desired. The pathological behavior of the fixed-order cross section for low p_T^{veto} is clear, as the central value becomes negative for $p_T^{veto} \approx 15$ GeV. This pathology is removed in the NLL$'$ + NLO result.

We continue by showing in Fig. 5 the cross section as a function of the lower cut on p_T^J for $p_T^{veto} = 30$ GeV. Even for values of the lower p_T^J cut near p_T^{veto}, a sizeable reduction of the uncertainty occurs when the NLL$'$ + NLO result is used. The reason for this is discussed in Sec. IV B; roughly half of the uncertainty comes from the high-p_T^J region, which is exactly the parameter space improved by our effective-theory description.

Finally, we present in Table I numerical results for both the cross sections and the fraction of events in the one-jet bin, f^{1j}. We define the event fraction as

$$f_x^{1j} = \frac{\sigma_x}{\sigma_{inc}}, \tag{32}$$

where x denotes either the NLO or the NLL$'$ + NLO cross section in the one-jet bin. We note that our values for f_{NLO}^{1j} are consistent with those obtained by the ATLAS collaboration [54], which provides a cross-check of our results.The total cross section σ_{inc}, as well as its estimated uncertainty, is taken from the LHC Higgs cross section working group [55]. The uncertainties shown are calculated as discussed in Sec. IV C. Results are given for $m_H = 124 - 126$ GeV, and for $p_T^{veto} = 25$ and 30 GeV. The reductions of the uncertainties are significant for both

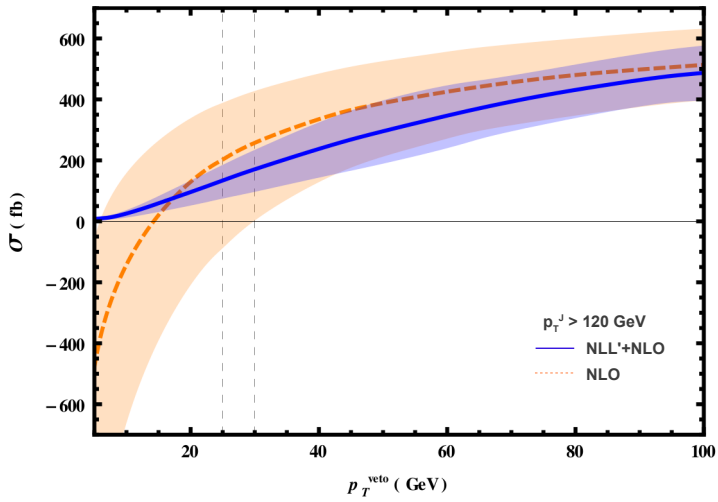

FIG. 4: Presented here are the NLO v.s. NLL′+NLO integrated cross sections with $p_T^J > 120\,\text{GeV}$. The blue solid line is for the RG-improved cross section and the yellow dashed line is the NLO prediction . The narrow blue band is obtained using Eq. (29) for the uncertainty after resummation, while the wide yellow band comes from using Eq. (28) for the fixed-order uncertainty.

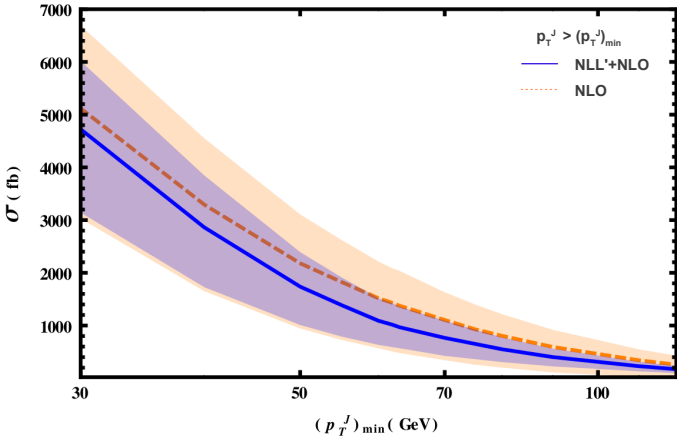

FIG. 5: Shown are the NLL′ + NLO (blue band) and NLO (yellow band) cross sections for fixed $p_T^{veto} = 30\,\text{GeV}$ as a function of the lower cut on p_T^J.

values of p_T^{veto}. Symmetrizing the error for this discussion, the estimated uncertainty on the cross section improves from ±40% at NLO to ±30% at NLL′ + NLO, a reduction of one quarter of the initial value. The one-jet fraction uncertainty decreases from ±44% to ±34%. For $p_T^{veto} = 30$ GeV, the error on the cross section decreases from ±36% to ±29% when

m_H (GeV)	p_T^{veto} (GeV)	$\sigma_{\rm NLO}$ (pb)	$\sigma_{\rm NLL'+NLO}$ (pb)	$f^{1j}_{\rm NLO}$	$f^{1j}_{\rm NLL'+NLO}$
124	25	$5.92^{+35\%}_{-46\%}$	$5.62^{+29\%}_{-30\%}$	$0.299^{+38\%}_{-49\%}$	$0.283^{+33\%}_{-34\%}$
125	25	$5.85^{+34\%}_{-46\%}$	$5.55^{+29\%}_{-30\%}$	$0.300^{+37\%}_{-49\%}$	$0.284^{+33\%}_{-33\%}$
126	25	$5.75^{+35\%}_{-46\%}$	$5.47^{+30\%}_{-30\%}$	$0.300^{+38\%}_{-49\%}$	$0.284^{+34\%}_{-33\%}$
124	30	$5.25^{+31\%}_{-41\%}$	$4.83^{+29\%}_{-29\%}$	$0.265^{+35\%}_{-43\%}$	$0.244^{+33\%}_{-33\%}$
125	30	$5.19^{+32\%}_{-41\%}$	$4.77^{+30\%}_{-29\%}$	$0.266^{+35\%}_{-43\%}$	$0.244^{+33\%}_{-33\%}$
126	30	$5.12^{+32\%}_{-41\%}$	$4.72^{+30\%}_{-29\%}$	$0.266^{+35\%}_{-43\%}$	$0.246^{+33\%}_{-32\%}$

TABLE I: Shown are the central values and uncertainties for the NLO cross section, the resummed cross section, and the event fractions in the one-jet bin using both the fixed-order and the resummed results. Numbers are given for several Higgs masses and for $p_T^{veto} = 25, 30$ GeV.

resummation is included, while the error on f^{1j} decreases from $\pm 39\%$ to $\pm 33\%$. Numerical results for other parameter choices are available from the authors upon request. We note that these are extremely conservative error estimates, as discussed in Sec. IV C. We default to the ST prescription over a large region of the relevant parameter space, and turn off the resummation at a relatively high value of p_T^J. Enough of the error comes from the high p_T^J region that our RG-improvement is effective in taming the uncertainty.

V. CONCLUSIONS

We have studied in detail the resummation of a class of large Sudakov logarithms appearing in the perturbative expansion for Higgs production in the one-jet bin. These logarithms occur when the jet transverse momentum is of order the Higgs mass. For certain parameter choices they lead to pathological behavior of the fixed-order perturbative expansions, including negative cross sections and scale-uncertainty estimates that do no properly account for missing higher-order corrections. Past attempts to handle this problem increased the theoretical error estimate. While theoretically correct, this has the unfortunate effect of introducing a large systematic error into experimental analyses. The results we present here tame the poor behavior of fixed-order QCD by controlling the jet-veto logarithms to all orders in perturbation theory, leading to a more reliable theoretical prediction and a reduced uncertainty estimate. We have reviewed the necessary formalism to understand the

resummation, and have extended the theoretical accuracy to the NLL$'$ level by calculating the full one-loop soft function for this process. Using our matched NLL$'$ + NLO result for the cross section, we have performed a detailed numerical study of exclusive Higgs plus one-jet production at the LHC, including an estimation of the non-global logarithmic effect and a careful accounting of the theoretical uncertainties before and after resummation. The estimated theoretical uncertainties in the one-jet bin are reduced by up to 25% using the NLL$'$ + NLO prediction. This is an extremely conservative error estimate, as argued in the main text.

We believe that it is now time to revisit the theoretical error treatment used by the LHC experiments in their studies of Higgs properties. Current studies use fixed-order perturbation theory, and the error treatment suggested in Ref. [32], to estimate the uncertainties induced by dividing the signal into exclusive jet multiplicites. While this is the best choice to correctly handle the uncertainties induced by the jet veto if only fixed-order predictions are available, the resummation of jet-veto logarithms is now known for both the zero-jet and one-jet bins. These predictions do not exhibit the pathological scale variation that led to the prescription of Ref. [32]. We are confident that this is only the first of many upcoming improvements for predictions of Higgs-boson production in association with a fixed number of jets. A new factorization theorem for the low-p_T^J region for exclusive Higgs plus one-jet production, an improved treatment of $\ln R$ effects, and new high-precision fixed-order calculations will all further reduce the theoretical uncertainties and help provide a sharpened image of the newly-discovered scalar at the LHC. We encourage the experimental communities to incorporate this new knowledge into their analyses.

Acknowledgments

We thank J. Qian and G. Salam for helpful discussions. This work was supported by the U.S. Department of Energy, Division of High Energy Physics, under contract DE-AC02-06CH11357 and the grants DE-FG02-95ER40896 and DE-FG02-08ER4153.

Appendix A: Fixed-order jet and beam functions

In this Appendix, we tabulate all ingredients needed for resummation at NLL$'$ accuracy. We start with the NLO calculation of the jet and the beam functions, whose operator definitions can be found in Ref. [44]. The anti-k_T jet function is calculated using the measurement function

$$\hat{\mathcal{M}}_J = \Theta(\Delta\eta_{ij}^2 + \Delta\phi_{ij}^2 < R^2) + \mathcal{O}(p_T^{veto})\,. \tag{A1}$$

We explicitly check that the collinear radiation leaking outside the jet is power-suppressed by p_T^{veto} after correctly subtracting the soft zero-bin contributions. Since numerically $R \ll 1$, we can simplify the measure using

$$\Delta\eta_{ij}^2 + \Delta\phi_{ij}^2 = 2\cosh(\Delta\eta_{ij}) - 2\cos(\Delta\phi_{ij}) + \mathcal{O}(R^4). \tag{A2}$$

In this limit, the NLO jet functions for gluons and quarks become

$$\begin{aligned}
J_g^{(1)} &= \frac{\alpha_s(\mu)}{2\pi}\left[C_A\left(\frac{67}{9} - \frac{3\pi^2}{4}\right) - \frac{23}{9}\frac{n_f}{2} + \beta_0 \log\frac{\mu}{p_T^J R} + 2C_A \log^2\frac{\mu}{p_T^J R}\right] + \mathcal{O}(R^2)\,,\\
J_q^{(1)} &= \frac{\alpha_s(\mu)}{2\pi}C_F\left[\frac{13}{2} - \frac{3\pi^2}{4} + 3\log\frac{\mu}{p_T^J R} + 2\log^2\frac{\mu}{p_T^J R}\right] + \mathcal{O}(R^2)\,,
\end{aligned} \tag{A3}$$

similar to what was obtained in Ref. [52] using a slightly different jet algorithm. We note that the jet functions are normalized so that the leading-order results are unity for both quarks and gluons: $J_i^{(0)} = 1$.

The measurement operator for the beam function with a single emission is

$$\hat{\mathcal{M}}_B = \Theta\left(k_{T,i} < p_T^{veto}\right)\,\Theta\left(|\eta_i| < \eta_{\rm cut}\right) + \Theta(|\eta_i| > \eta_{\rm cut})\,. \tag{A4}$$

Experimentally, $\eta_{\rm cut} \sim 4.5$. For simplicity, we set $\eta_{\rm cut} = \infty$ here. We note that this difference does not affect the anomalous dimension of the beam function, it only changes the finite part. The calculation is performed using the 't Hooft-Veltmann scheme. The NLO matching coefficient $\mathcal{I}$ for the various beam functions are found to be

$$\begin{aligned}
\mathcal{I}_{gg}^{(1)}(z) &= \frac{\alpha_s(\mu)C_A}{2\pi}\left(4\log\frac{\mu}{p_T^{veto}}\log\frac{\nu}{\bar{n}\cdot p}\delta(1-z) - 2\tilde{p}_{gg}(z)\log\frac{\mu}{p_T^{veto}}\right)\,,\\
\mathcal{I}_{qq}^{(1)}(z) &= \frac{\alpha_s(\mu)C_F}{2\pi}\left(4\log\frac{\mu}{p_T^{veto}}\log\frac{\nu}{\bar{n}\cdot p}\delta(1-z) - 2\tilde{p}_{qq}(z)\log\frac{\mu}{p_T^{veto}} + (1-z)\right)\,,\\
\mathcal{I}_{gq}^{(1)}(z) &= \frac{\alpha_s(\mu)C_F}{2\pi}\left(-2p_{gq}(z)\log\frac{\mu}{p_T^{veto}} + z\right)\,,\\
\mathcal{I}_{qg}^{(1)}(z) &= \frac{\alpha_s(\mu)T_F}{2\pi}\left(-2p_{qg}(z)\log\frac{\mu}{p_T^{veto}} + 2z(1-z)\right)\,,
\end{aligned} \tag{A5}$$

with

$$\tilde{p}_{gg}(z) = \frac{2z}{(1-z)_+} + 2z(1-z) + 2\frac{1-z}{z}\,,$$
$$\tilde{p}_{qq}(z) = \frac{1+z^2}{(1-z)_+}\,,$$
$$p_{gq}(z) = \frac{1+(1-z)^2}{z}\,,$$
$$p_{qg}(z) = 1 - 2z + 2z^2\,. \tag{A6}$$

We note that the beam functions are normalized so that the diagonal matching coefficients are delta-functions at tree-level, while the off-diagonal ones vanish: $\mathcal{I}_{ii}^{(0)} = \delta(1-z)$, $\mathcal{I}_{ij}^{(0)} = 0$ for $i \neq j$.

Appendix B: Anomalous dimensions and RG evolution

The beam, jet, soft and hard functions appearing in the factorization theorem of Eq. (5) all satisfy evolution equations of the form

$$\mu\frac{\mathrm{d}F}{\mathrm{d}\mu} = \Gamma_F^{\mu}(\mu)F(\mu)\,. \tag{B1}$$

The soft and beam functions, which also contain rapidity divergences, have similar evolution equations in the rapidity regulator:

$$\nu\frac{\mathrm{d}F_{B,S}}{\mathrm{d}\nu} = \Gamma_{B,S}^{\nu}(\nu)F_{B,S}(\nu)\,. \tag{B2}$$

These are easily extracted form the poles of the one-loop calculations for each of these objects. The general solution to these RG equations can be formally written as

$$F(\mu,\nu) = U(\mu,\nu,\mu_0,\nu_0)F(\mu_0,\nu_0)\,. \tag{B3}$$

These RG-improved expressions for the beam, soft, jet and hard functions are then used in Eq. (5). The initial conditions in Eq. (B3) can be determined from the fixed-order calculation presented in the previous section and in the main text for the soft function.

From these fixed order calculations, we can determine the anomalous dimensions used for RG evolution. The anomalous dimension for the jet function is given by

$$\Gamma_{J_i} = 2\Gamma_{\mathrm{cusp}}T_i^2\log\frac{\mu}{p_T^{J_i}R} + \gamma_{J_i}\,. \tag{B4}$$

Here, i labels the parton flavor, and can take on the values $i = q, g$. For the beam function, the anomalous dimensions are

$$\begin{aligned}\Gamma_B^\nu &= 2\Gamma_{\rm cusp} T_i^2 \log\frac{\mu}{p_T^{veto}}\,,\\ \Gamma_B^\mu &= 2\Gamma_{\rm cusp} T_i^2 \log\frac{\nu}{\bar{n}\cdot p} + \gamma_{B_i}\,,\end{aligned} \tag{B5}$$

where $T_i^2 = C_A$ for gluon and $T_i^2 = C_F$ for quark. The anomalous dimensions can be obtained as expansions in the strong coupling constant. For the resummation performed here, we need the following terms in each expansion:

$$\begin{aligned}\Gamma_{\rm cusp} &= \frac{\alpha_s}{4\pi}\Gamma_0 + \left(\frac{\alpha_s}{4\pi}\right)^2\Gamma_1 + \ldots,\\ \gamma_{B_i} &= \frac{\alpha_s}{4\pi}\gamma_0^i,\quad \gamma_{J_i} = \frac{\alpha_s}{4\pi}\gamma_0^i.\end{aligned} \tag{B6}$$

We note that the non-cusp anomalous dimensions of the beam and jet functions are the same. We have the following expressions for the necessary anomalous dimensions, as well as the relevant coefficients of the QCD beta functions needed both here and later:

$$\begin{aligned}&\beta_0 = \frac{11}{3}C_A - \frac{4}{3}T_F n_f\,,\\ &\beta_1 = \frac{34}{3}C_A^2 - \frac{20}{3}C_A T_F n_f - 4C_F T_F n_f\,,\\ &\Gamma_0 = 4\,,\\ &\Gamma_1 = 4\left[C_A\left(\frac{67}{9} - \frac{\pi^2}{3}\right) - \frac{20}{9}T_F n_f\right]\,,\\ &\gamma_0^g = 2\beta_0,\quad \gamma_0^q = 6C_F.\end{aligned} \tag{B7}$$

The RG evolution of the soft function can be easily obtained by direct differentiation of Eq. (20). As the soft function is sensitive to both the jet and beam directions, its anomalous dimensions take on a more complicated form than those of the other quantities. We find

$$\begin{aligned}\Gamma_S^\mu &= 2\Gamma_{\rm cusp}\left\{(T_a^2 + T_b^2)\ln\frac{\mu}{\nu} + y_J(T_a\cdot T_J - T_b\cdot T_J)\ln\frac{\mu}{p_T^{veto}}\right\},\\ \Gamma_S^\nu &= -2\Gamma_{\rm cusp}\left(T_a^2 + T_b^2\right)\ln\frac{\mu}{p_T^{veto}},\end{aligned} \tag{B8}$$

where a, b denote the beam directions and J the final-state jet direction. We note that $\Gamma_S^\nu + \Gamma_{B_a}^\nu + \Gamma_{B_b}^\nu = 0$, as required by RG-invariance of the cross section under ν-variations. The anomalous dimension of the hard function was studied in detail in Ref. [53], and we do not reproduce it here. It can be derived from the above expression using RG-invariance of the cross section: $\Gamma_S^\mu + \Gamma_{B_a}^\mu + \Gamma_{B_b}^\mu + \Gamma_J^\mu + \Gamma_H^\mu = 0$.

Appendix C: Solutions of the RG equations

We reproduce here the solutions to the RG equations presented in the previous section, which are required in Eq. (B3). The evolutions of the jet and the beam functions are given by

$$\begin{aligned} U_{J_i}(\mu_J,\mu) &= \exp\left[-2T_i^2 S(\mu_J,\mu) - A_{J_i}(\mu_J,\mu)\right]\left(\frac{\mu_J}{p_T^J R}\right)^{-2T_J^2 A_\Gamma(\mu_J,\mu)}, \\ U_{B,a}(\mu_B,\nu_B,\mu,\nu) &= \exp\left[-T_a^2 A_\Gamma(p_T^{veto},\mu)\log\frac{\nu^2}{\nu_B^2}\right]\exp\left[-T_a^2 A_\Gamma(\mu_B,\mu)\log\frac{\nu_B^2}{\omega_a^2} - A_{B_a}(\mu_B,\mu)\right]. \end{aligned} \tag{C1}$$

The solution to the RG equation for the hard function is is

$$\begin{aligned} U_H(\mu_H,\mu) &= \exp\left[2\sum_i T_i^2 S(\mu_H,\mu) - 2A_H(\mu_H,\mu) + 2A_\Gamma(\mu_H,\mu)\sum_{i\neq j}\frac{T_i\cdot T_j}{2}\log\Delta R_{ij}^2\right] \\ &\quad\times\prod_i\left(\frac{\mu_H}{\omega_i}\right)^{2T_i^2 A_\Gamma(\mu_H,\mu)}, \end{aligned} \tag{C2}$$

where we have set $\Delta R_{Ja}^2 = e^{-\eta_J}$, $\Delta R_{Jb}^2 = e^{\eta_J}$ and $\Delta R_{ab}^2 = 1$. We also set $\omega_i = p_T^J$ if $i = J$, otherwise we have $\omega_a = x_a\sqrt{s}$. The soft-function evolution factor is

$$\begin{aligned} U_S(\mu_S,\nu_S,\mu,\nu) &= \exp\left[-2\sum_{i\in B} T_i^2 S(\mu_s,\mu) - A_s(\mu_s,\mu) - 2A_\Gamma(\mu_s,\mu)\sum_{i\neq j}\frac{T_i\cdot T_j}{2}\log\Delta R_{ij}^2\right] \\ &\quad\times\left(\frac{1}{R}\right)^{2T_J^2 A_\Gamma(\mu_s,\mu)}\left(\frac{\nu_s}{\mu_s}\right)^{\sum_{i\in B}2T_i^2 A_\Gamma(\mu_s,\mu)}\left(\frac{\nu}{\nu_s}\right)^{\sum_{i\in B}2T_i^2 A_\Gamma(p_T^{veto},\mu)}. \end{aligned} \tag{C3}$$

For the NLL resummation, we need the following factors:

$$A_\Gamma(\mu_i,\mu_f) = \frac{\Gamma_0}{2\beta_0}\left\{\log r + \frac{\alpha_s(\mu_i)}{4\pi}\left(\frac{\Gamma_1}{\Gamma_0} - \frac{\beta_1}{\beta_0}\right)(r-1)\right\}, \tag{C4}$$

and

$$S(\mu_i,\mu_f) = \frac{\Gamma_0}{4\beta_0^2}\left\{\frac{4\pi}{\alpha_s(\mu_i)}\left(1 - \frac{1}{r} - \log r\right) + \left(\frac{\Gamma_1}{\Gamma_0} - \frac{\beta_1}{\beta_0}\right)(1 - r + \log r) + \frac{\beta_1}{2\beta_0}\log^2 r\right\}, \tag{C5}$$

where $r = \alpha_s(\mu_f)/\alpha_s(\mu_i)$. $A_{J/B}$, A_H and A_S are needed at leading order, and can be obtained by substituting the Γ_0 in A_Γ with the corresponding γ_0^i and expanding in α_s.

---

[1] G. Aad *et al.* [ATLAS Collaboration], Phys. Lett. B **716**, 1 (2012) [arXiv:1207.7214 [hep-ex]].

[2] S. Chatrchyan *et al.* [CMS Collaboration], Phys. Lett. B **716**, 30 (2012) [arXiv:1207.7235 [hep-ex]].

[3] ATLAS Collaboration, ATLAS-CONF-2012-170.

[4] S. Chatrchyan *et al.* [CMS Collaboration], arXiv:1212.6639 [hep-ex].

[5] S. Dawson, Nucl. Phys. B **359**, 283 (1991).

[6] A. Djouadi, M. Spira and P. M. Zerwas, Phys. Lett. B **264**, 440 (1991).

[7] M. Spira, A. Djouadi, D. Graudenz and P. M. Zerwas, Nucl. Phys. B **453**, 17 (1995) [hep-ph/9504378].

[8] D. de Florian, M. Grazzini and Z. Kunszt, Phys. Rev. Lett. **82**, 5209 (1999) [hep-ph/9902483].

[9] V. Ravindran, J. Smith and W. L. Van Neerven, Nucl. Phys. B **634**, 247 (2002) [hep-ph/0201114].

[10] C. J. Glosser and C. R. Schmidt, JHEP **0212**, 016 (2002) [hep-ph/0209248].

[11] J. M. Campbell, R. K. Ellis and G. Zanderighi, JHEP **0610**, 028 (2006) [hep-ph/0608194].

[12] R. V. Harlander and W. B. Kilgore, Phys. Rev. Lett. **88**, 201801 (2002) [hep-ph/0201206].

[13] C. Anastasiou and K. Melnikov, Nucl. Phys. B **646**, 220 (2002) [hep-ph/0207004].

[14] V. Ravindran, J. Smith and W. L. van Neerven, Nucl. Phys. B **665**, 325 (2003) [hep-ph/0302135].

[15] C. Anastasiou, K. Melnikov and F. Petriello, Phys. Rev. Lett. **93**, 262002 (2004) [hep-ph/0409088].

[16] C. Anastasiou, K. Melnikov and F. Petriello, Nucl. Phys. B **724**, 197 (2005) [hep-ph/0501130].

[17] C. Anastasiou, G. Dissertori and F. Stockli, JHEP **0709**, 018 (2007) [arXiv:0707.2373 [hep-ph]].

[18] S. Catani and M. Grazzini, Phys. Rev. Lett. **98**, 222002 (2007) [hep-ph/0703012].

[19] M. Grazzini, JHEP **0802**, 043 (2008) [arXiv:0801.3232 [hep-ph]].

[20] R. Boughezal, F. Caola, K. Melnikov, F. Petriello and M. Schulze, arXiv:1302.6216 [hep-ph].

[21] U. Aglietti, R. Bonciani, G. Degrassi and A. Vicini, Phys. Lett. B **595**, 432 (2004) [hep-ph/0404071].

[22] S. Actis, G. Passarino, C. Sturm and S. Uccirati, Phys. Lett. B **670**, 12 (2008) [arXiv:0809.1301 [hep-ph]].

[23] C. Anastasiou, R. Boughezal and F. Petriello, JHEP **0904**, 003 (2009) [arXiv:0811.3458 [hep-ph]].

[24] R. Boughezal, arXiv:0908.3641 [hep-ph].

[25] S. Dittmaier *et al.* [LHC Higgs Cross Section Working Group Collaboration], arXiv:1101.0593 [hep-ph].

[26] S. Dittmaier, S. Dittmaier, C. Mariotti, G. Passarino, R. Tanaka, S. Alekhin, J. Alwall and E. A. Bagnaschi *et al.*, arXiv:1201.3084 [hep-ph].

[27] M. Grazzini, EPJ Web Conf. **28**, 07001 (2012) [arXiv:1202.3927 [hep-ph]].

[28] G. Aad *et al.* [ATLAS Collaboration], Phys. Lett. B **716**, 62 (2012) [arXiv:1206.0756 [hep-ex]].

[29] S. Chatrchyan *et al.* [CMS Collaboration], Phys. Lett. B **710**, 91 (2012) [arXiv:1202.1489 [hep-ex]].

[30] A. Banfi, G. P. Salam and G. Zanderighi, JHEP **1206**, 159 (2012) [arXiv:1203.5773 [hep-ph]].

[31] C. Anastasiou, G. Dissertori, F. Stockli and B. R. Webber, JHEP **0803**, 017 (2008) [arXiv:0801.2682 [hep-ph]].

[32] I. W. Stewart and F. J. Tackmann, Phys. Rev. D **85**, 034011 (2012) [arXiv:1107.2117 [hep-ph]].

[33] C. F. Berger, C. Marcantonini, I. W. Stewart, F. J. Tackmann and W. J. Waalewijn, JHEP **1104**, 092 (2011) [arXiv:1012.4480 [hep-ph]].

[34] S. Gangal and F. J. Tackmann, arXiv:1302.5437 [hep-ph].

[35] T. Becher and M. Neubert, JHEP **1207**, 108 (2012) [arXiv:1205.3806 [hep-ph]].

[36] A. Banfi, P. F. Monni, G. P. Salam and G. Zanderighi, arXiv:1206.4998 [hep-ph].

[37] F. J. Tackmann, J. R. Walsh and S. Zuberi, arXiv:1206.4312 [hep-ph].

[38] See the talk by J. Qian at the KITP workshop on Higgs identification, available at `http://online.kitp.ucsb.edu/online/higgs_m12/qian/`.

[39] C. W. Bauer, S. Fleming and M. E. Luke, Phys. Rev. D **63**, 014006 (2000) [hep-ph/0005275].

[40] C. W. Bauer, S. Fleming, D. Pirjol, and I. W. Stewart, Phys. Rev. **D63**, 114020 (2001), hep-ph/0011336.

[41] C. W. Bauer and I. W. Stewart, Phys. Lett. B **516**, 134 (2001) [hep-ph/0107001].

[42] C. W. Bauer, D. Pirjol, and I. W. Stewart, Phys. Rev. **D65**, 054022 (2002), hep-ph/0109045.

[43] C. W. Bauer, S. Fleming, D. Pirjol, I. Z. Rothstein, and I. W. Stewart, Phys. Rev. **D66**, 014017 (2002), hep-ph/0202088.

[44] X. Liu and F. Petriello, Phys. Rev. D **87**, 014018 (2013) [arXiv:1210.1906 [hep-ph]].

[45] M. Cacciari, G. P. Salam and G. Soyez, JHEP **0804**, 063 (2008) [arXiv:0802.1189 [hep-ph]].

[46] R. Kelley, J. R. Walsh and S. Zuberi, JHEP **1209**, 117 (2012) [arXiv:1202.2361 [hep-ph]].

[47] C. R. Schmidt, Phys. Lett. B **413**, 391 (1997) [hep-ph/9707448].

[48] M. Dasgupta and G. P. Salam, Phys. Lett. B **512**, 323 (2001) [hep-ph/0104277].

[49] J. -Y. Chiu, A. Jain, D. Neill and I. Z. Rothstein, JHEP **1205**, 084 (2012) [arXiv:1202.0814 [hep-ph]].

[50] J. M. Campbell and R. K. Ellis, Nucl. Phys. Proc. Suppl. **205-206**, 10 (2010) [arXiv:1007.3492 [hep-ph]].

[51] A. D. Martin, W. J. Stirling, R. S. Thorne and G. Watt, Eur. Phys. J. C **64**, 653 (2009) [arXiv:0905.3531 [hep-ph]].

[52] S. D. Ellis, C. K. Vermilion, J. R. Walsh, A. Hornig and C. Lee, JHEP **1011**, 101 (2010) [arXiv:1001.0014 [hep-ph]].

[53] R. Kelley and M. D. Schwartz, Phys. Rev. D **83**, 045022 (2011) [arXiv:1008.2759 [hep-ph]].

[54] Jianming Qian, private communication.

[55] `https://twiki.cern.ch/twiki/bin/view/LHCPhysics/CrossSections`